To be submitted to ACS Applied Materials & Interfaces

Supplementary Information

for

Non-Dendritic Zn Electrodeposition Enabled by Zincophilic Graphene Substrate

Tara Foroozan, Vitaliy Yurkiv, Soroosh Sharifi-Asl, Ramin Rojaee, Farzad Mashayek, Reza Shahbazian-Yassar*

Mechanical and Industrial Engineering Department, University of Illinois at Chicago, Chicago, Illinois 60607, United States.

*Correspondence to: rsyassar@uic.edu

Experimental results:

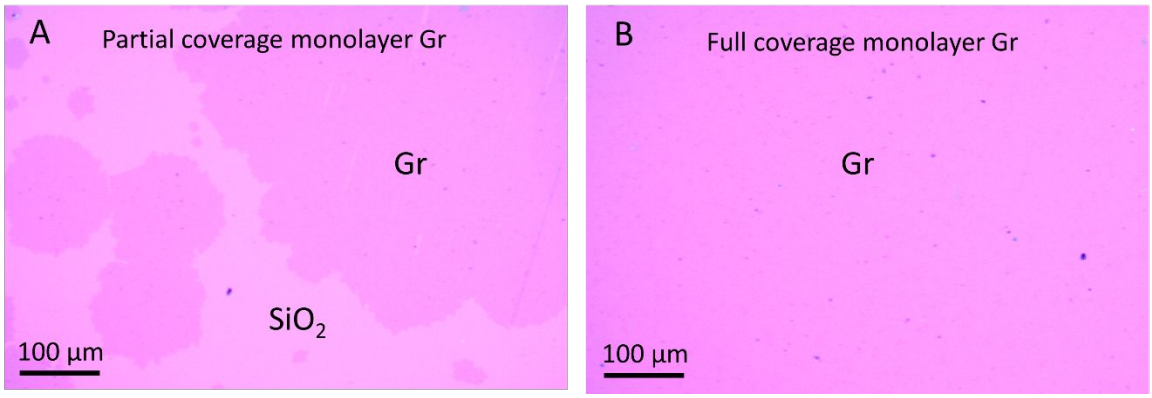

Figure S1. Optical image obtained from (A) Partial coverage (30 mins of CVD growth) and (B) Full coverage (40 mins of CVD growth) monolayer Gr transferred on Si/SiO_2 substrate.

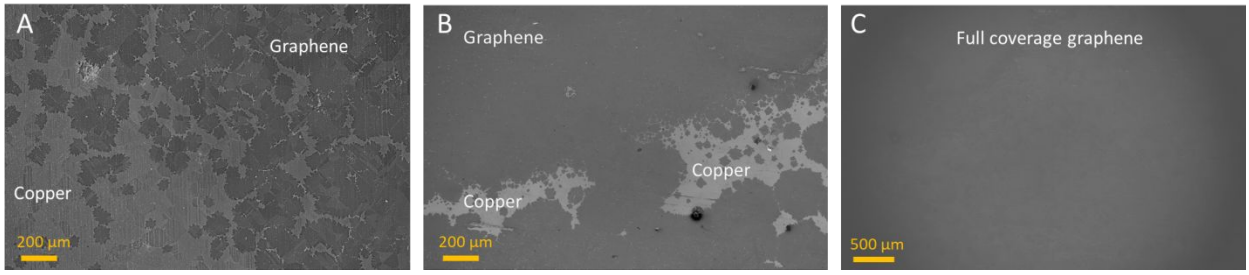

Figure S2. SEM images obtained after (A) 20 mins (B) 30 mins and (C) 40 mins of CVD growth of Gr on Cu surface.

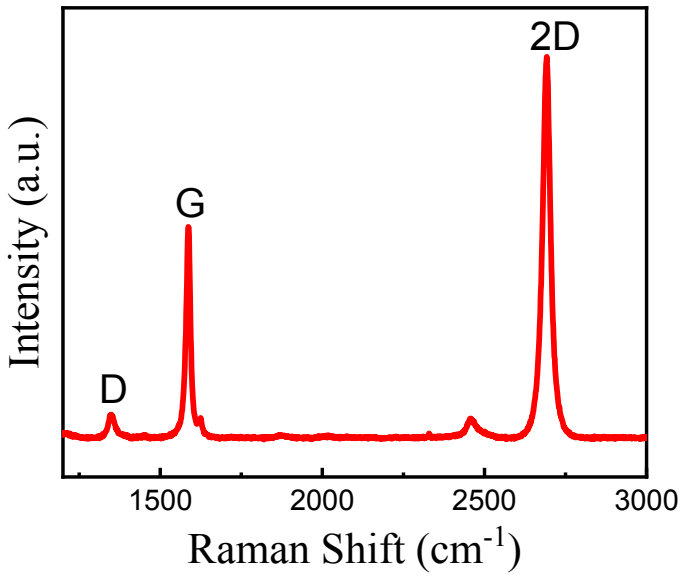

Figure S3. Raman spectra of single layer CVD grown graphene transferred on Si/SiO_2 substrate.

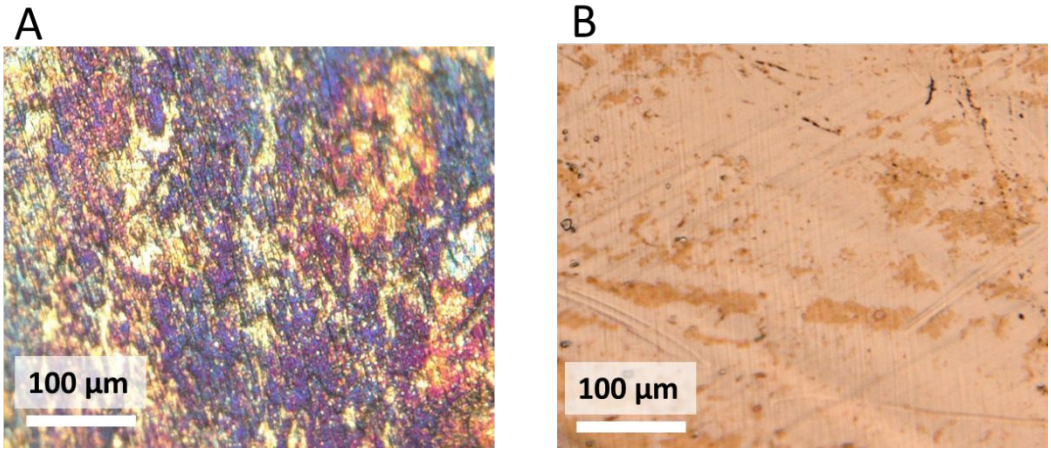

Figure S4. Optical microscopy image obtained from (A) bare and (B) Gr-modified electrodes at the full dissolution state after 30 cycling.

XPS data obtained from the surface of bare and Gr-modified electrode after 50 cycles at the discharged state is shown in Figure S5. Survey XPS result in Figure S5A shows that the Zn and O peaks have higher intensity in bare sample compared to Gr-modified electrode. The large amount of Zn detected in the brownish film confirms the irreversible Zn loss during cycling, which leads to lower CE% even from initial cycles shown in the inset of Figure 1C. The large oxygen peak detected on the surface of bare Cu, can be attributed to copper or zinc oxides. Figure S5B shows the binding energy in the carbon range, confirming the survival of graphene layer on the Cu surface even after prolonged cycling and suggests the Zn deposition on top of Gr and not in between Gr and Cu surface (see Figure 5 for further analysis). Figure S5C shows the lower amount of oxygen in the Gr-modified samples, which confirms the diminished side reactions achieved by using Gr as substrate. The shift in the Zn2p3 peaks (Figure S5D) confirms the existence of zinc oxide and the shoulder peak observed in the CuLM2 (Figure S5E) confirms the existence of copper oxide in the film formed on the surface of bare Cu.

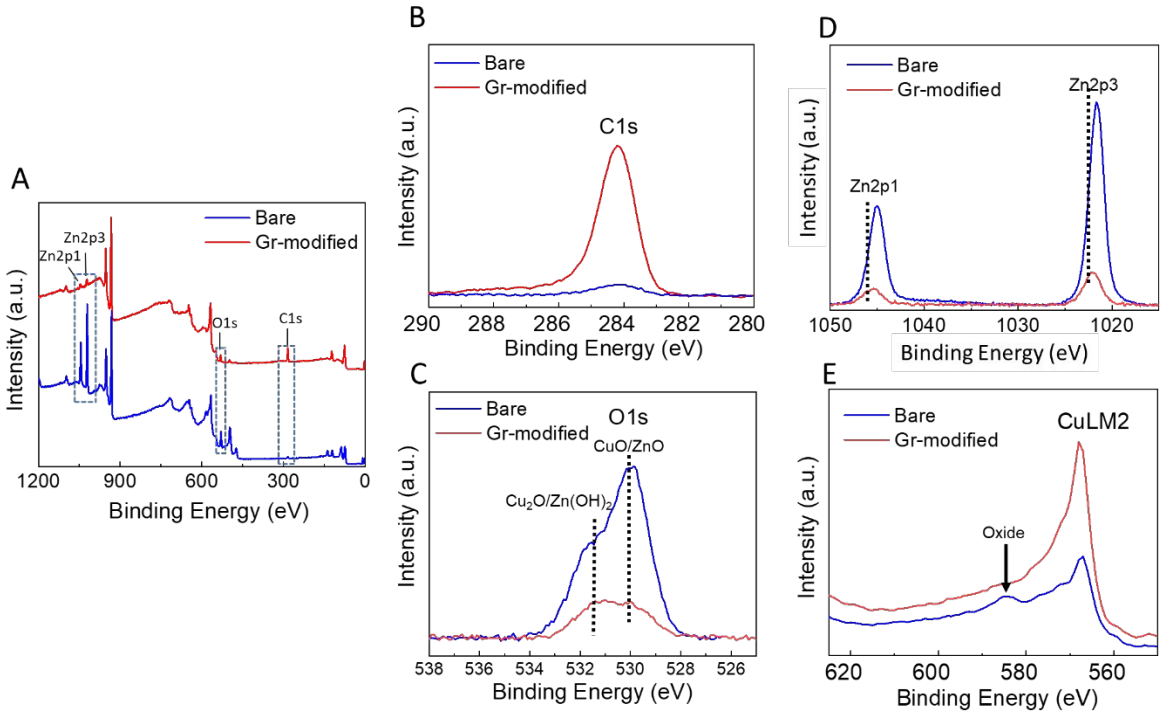

Figure S5. XPS data analysis on the surface of bare and Gr-modified Cu after full Zn stripping. (A) Survey spectra. High resolution spectra for (B) carbon (C) zinc (D) oxygen and (E) copper elements.

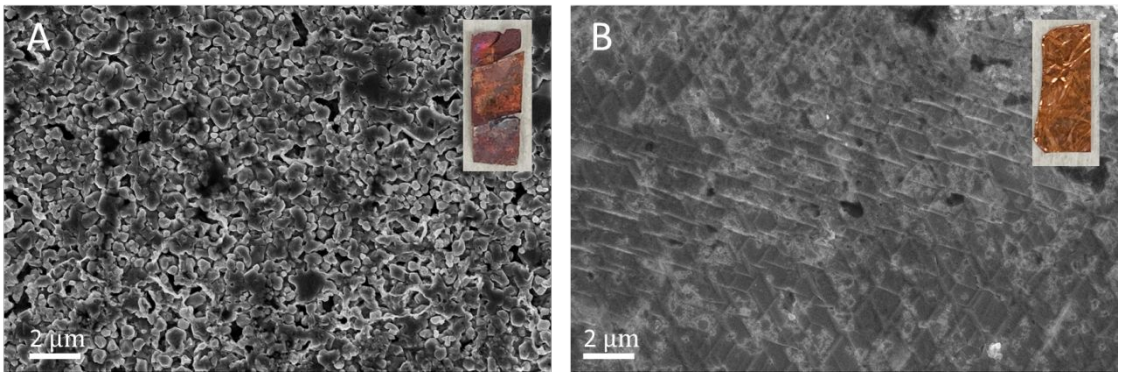

Figure S6. SEM and optical (inset) imaging obtained from (A) bare and (B) Gr-modified Cu electrodes after being soaked in 2M $ZnSO_4$ electrolyte for 30 days.

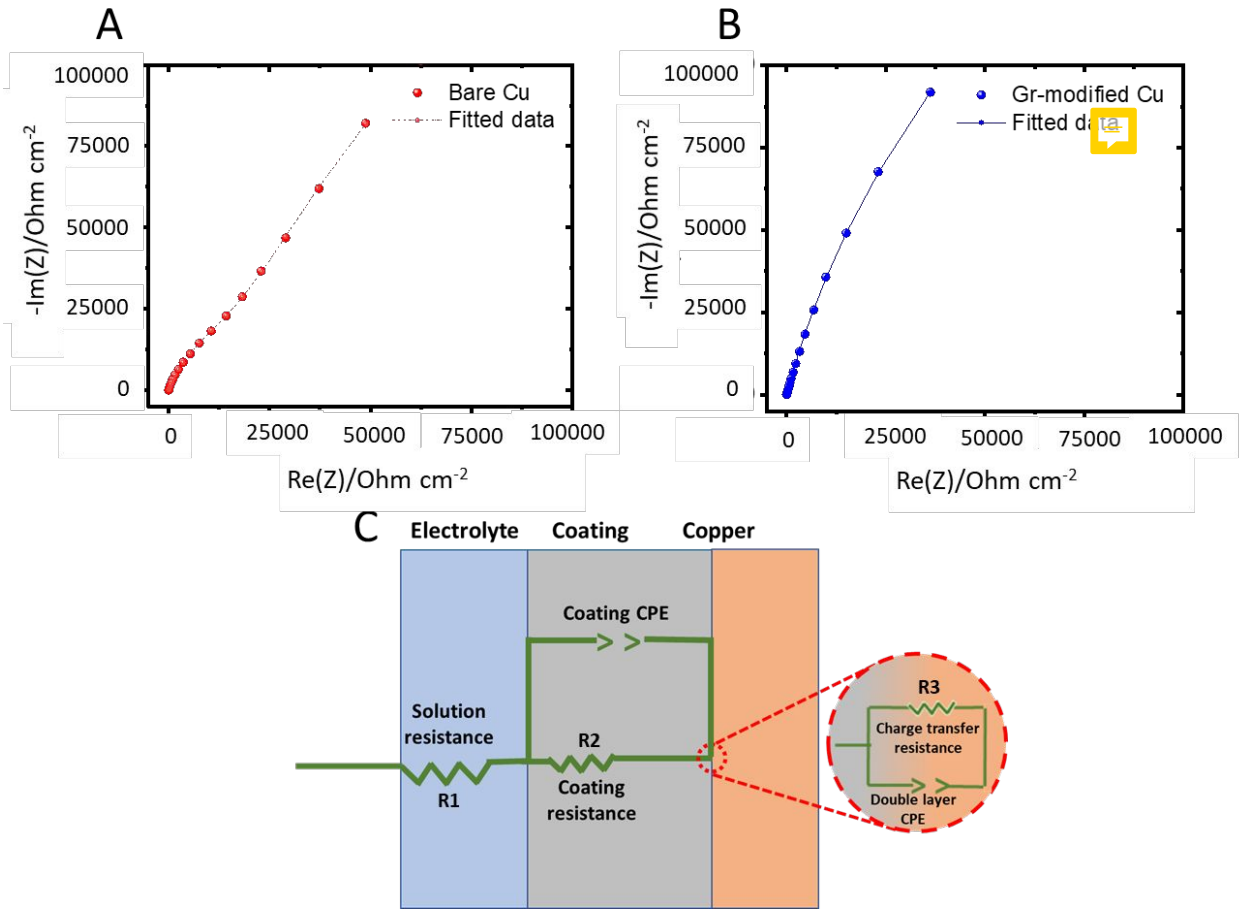

Figure S7. Nyquist plots of (A) bare and (B) graphene-modified electrodes and (C) the equivalent circuit model for Gr-modified electrode.

Table S1- Calculated parameters of the proposed EEC for the graphene coated and uncoated specimens.

	R_1 (Ω cm^{-2})	R_2 ($\times 10^3$ Ω cm^{-2})	R_3 ($\times 10^6$ Ω cm^{-2})
Bare Cu	11	50	509
Gr-modified Cu	12	72	534

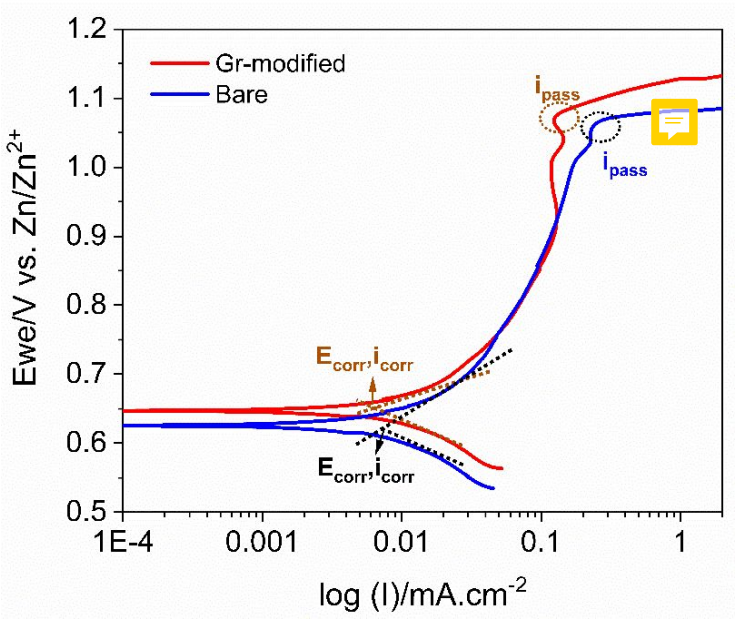

Figure S8. Tafel polarization curves for bare and Gr-modified Cu electrodes in 2M $ZnSO_4$ electrolyte.

Table S2- Mean values of corrosion current densities and potentials of bare, and Gr-modified Cu electrodes.

	E_{OCV} (mV)	E_{corr} (mV)	i_{corr} (μA.cm^{-2})	i_{pass} (μA.cm^{-2})
Pristine Cu	623	628	4.3	237
Gr-Cu	646	649	3.7	124

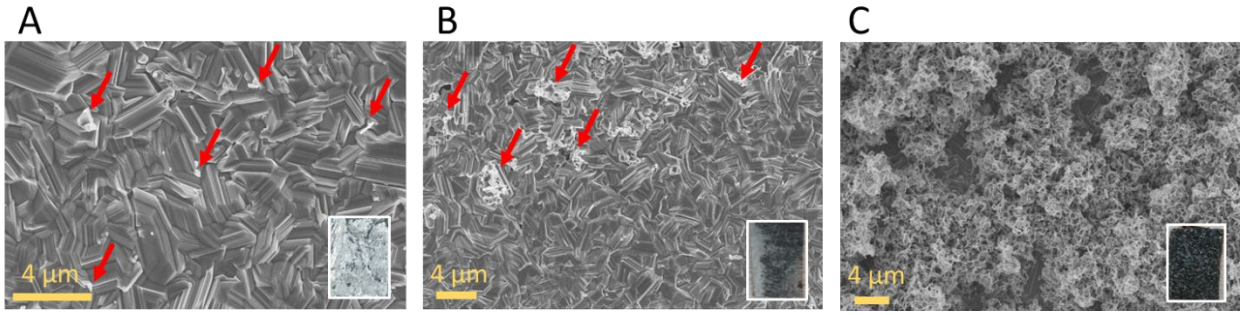

Figure S9. Development of Zn dendrites on top of Zn boulders by increasing the deposition time (Zn deposition capacity of 3, 6 and 10 mAh/cm^2 for A to C, respectively). Insets show corresponding optical images.

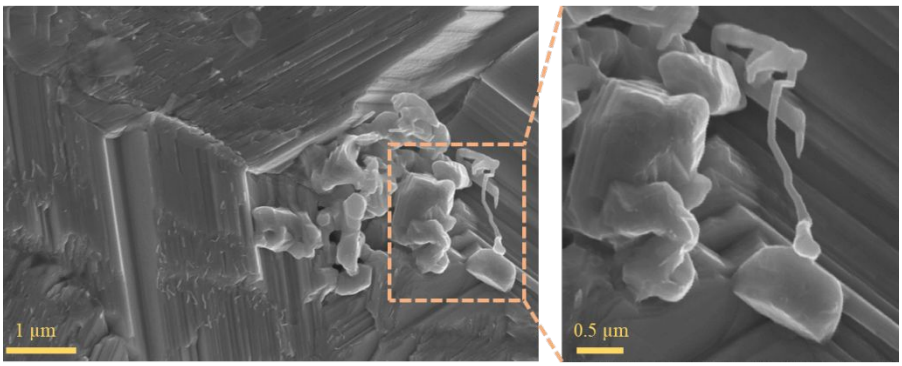

Figure S10. Initiation of Zn dendrites on top of Zn boulder's edge sites.

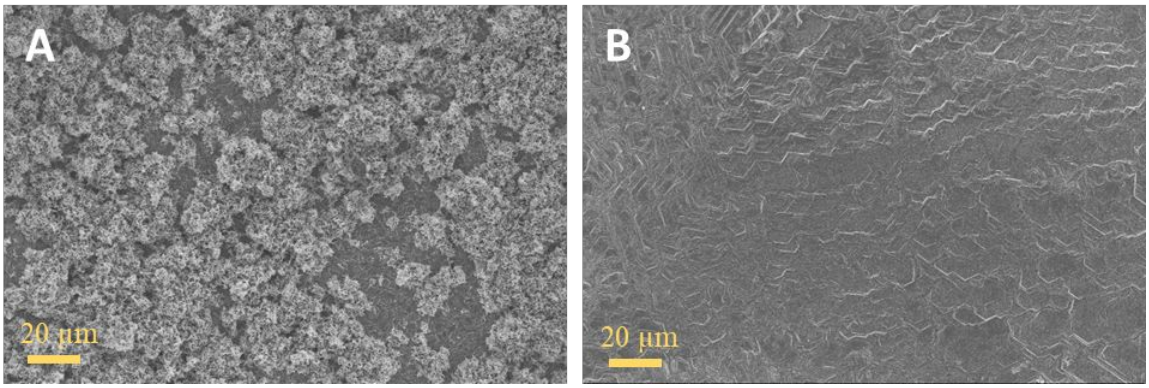

Figure S11. Low magnification SEM image obtained from Zn electrodeposited on (A) bare and (B) Gr-modified electrodes.

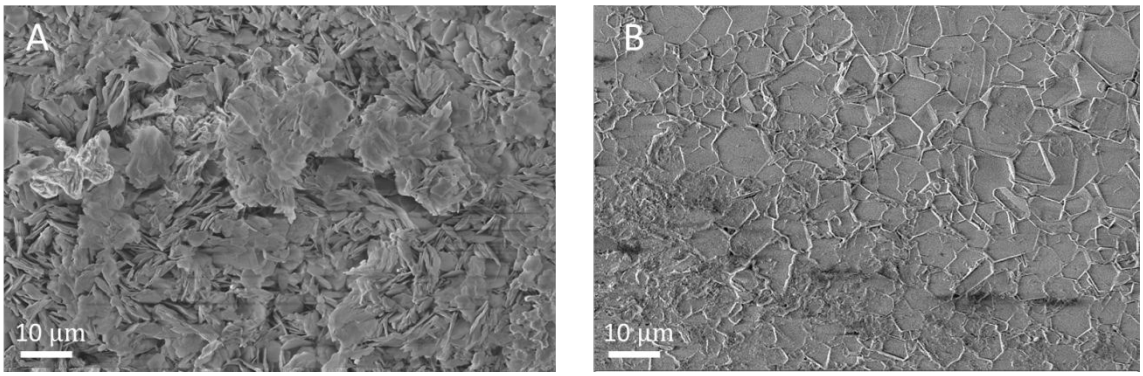

Figure S12. Zn morphological evolution after 30 cycles at the charged state for (A) bare and (B) Gr-modified electrod

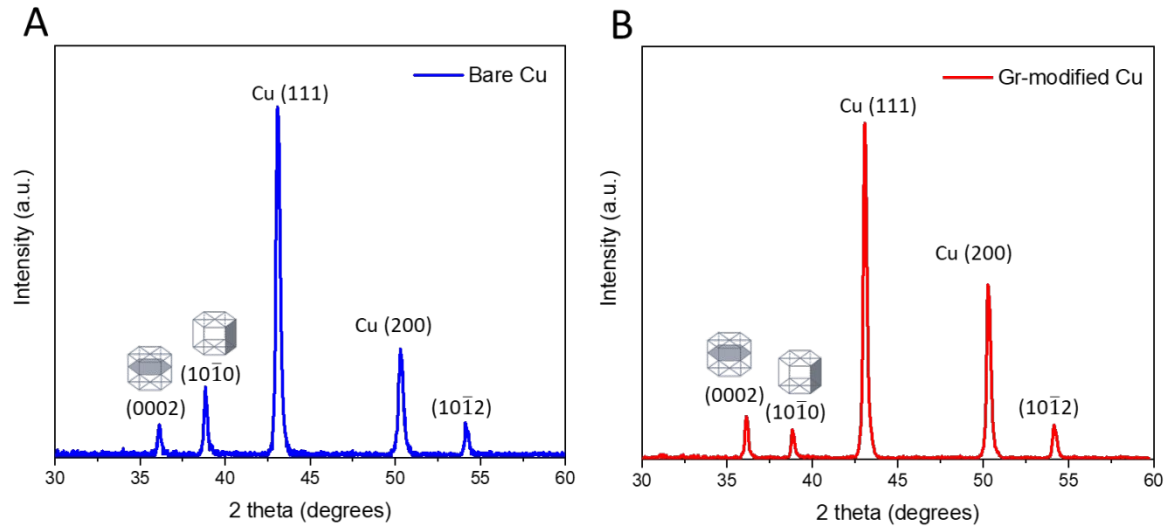

Figure S13. GIXRD pattern obtained from (a) bare and (b) Gr-modified Cu after 30 cycles at the charged state.

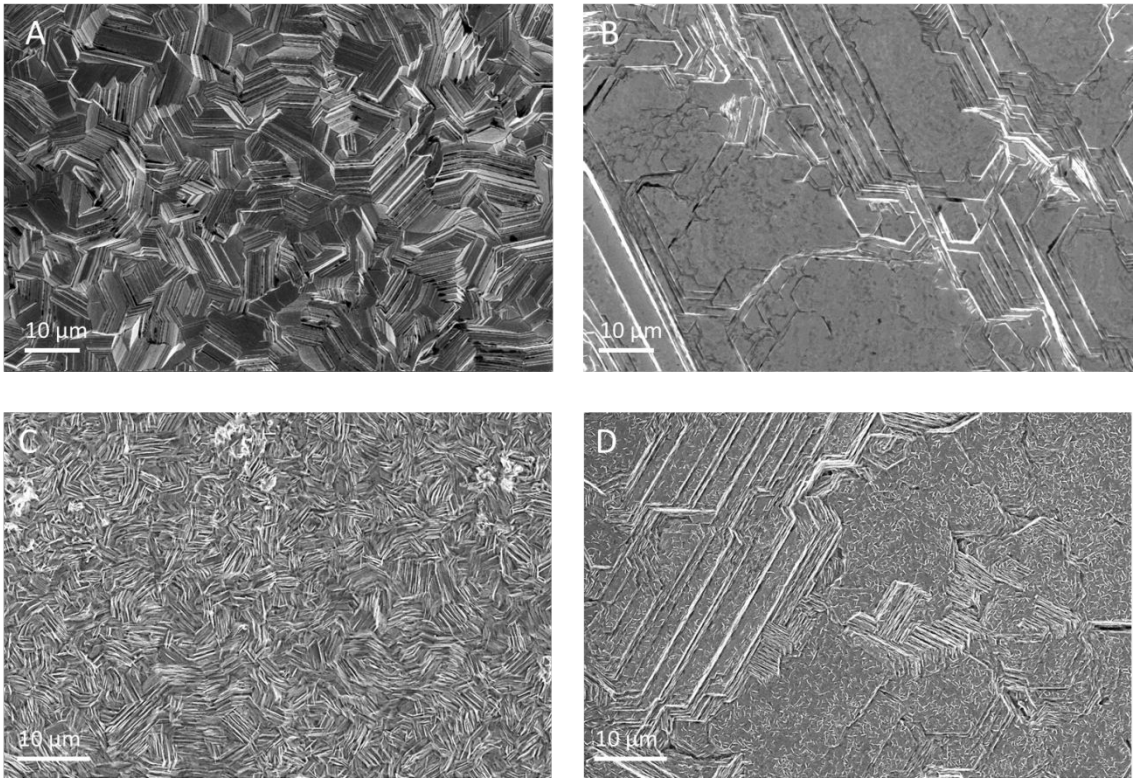

Figure S14. SEM images obtained from Zn electrodeposition on (a and c) bare and (b and d) Gr-modified Cu at current densities of (a and b) 10 mA/cm² and (c and d) 15 mA/cm². The deposition capacity is 5mAh/cm².

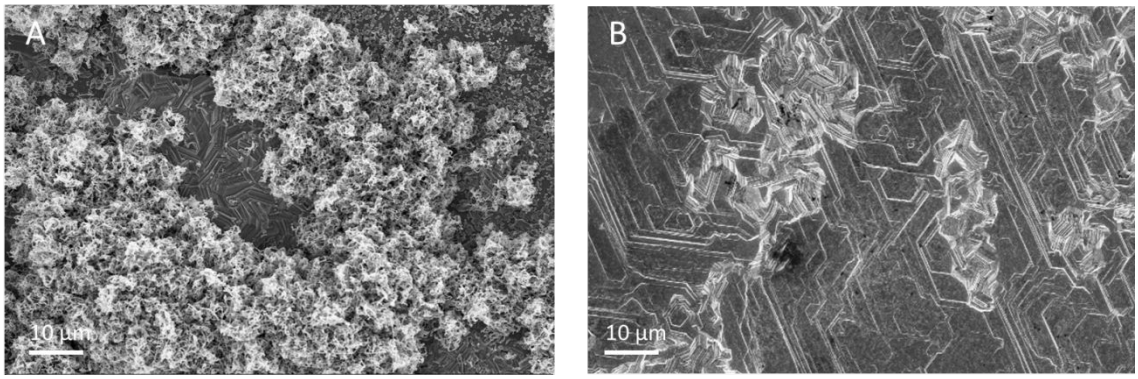

Figure S15. SEM images obtained from Zn electrodeposition on (a) bare and (b) Gr-modified Cu at current density of 2 mA/cm² . The deposition capacity is 2mAh/cm².

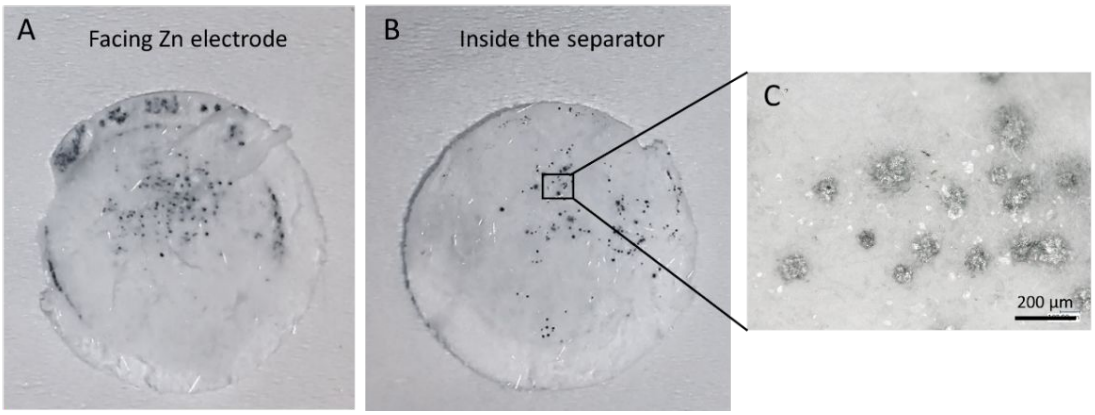

Figure S16. Zn dendrites penetration through the separator shown on (A) Zn facing and (B) inside the separator. (C) Magnified optical image of the dendrites punctured the separator.

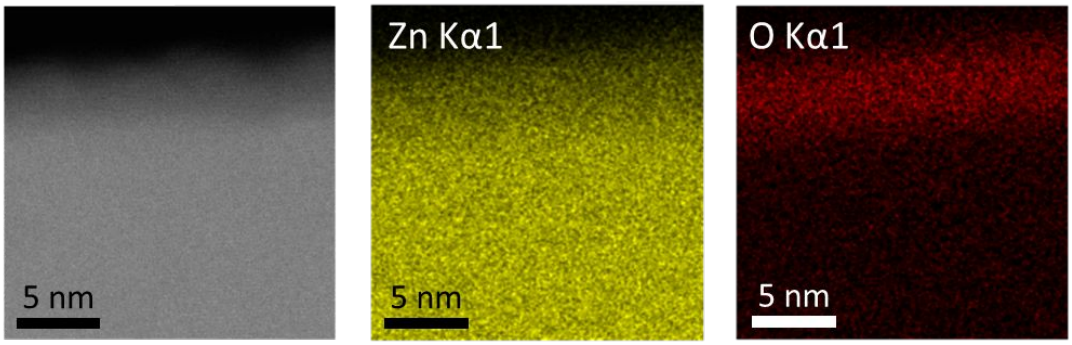

Figure S17. EDS map obtained from the surface of Zn electrodeposits showing the existence of thin oxide layer at the very top surface.

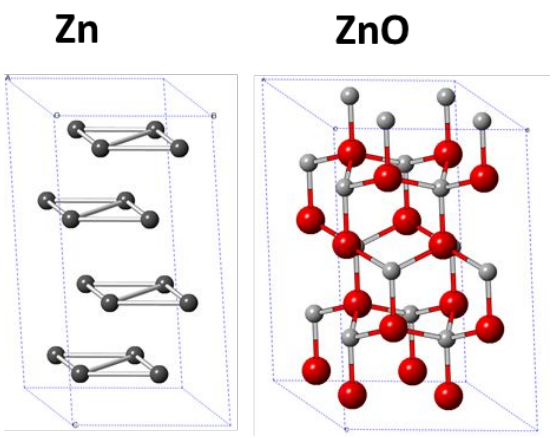

Figure S18. Unit cell models for hexagonal $P6_3/mmc$ Zn and hexagonal $P6_3mc$ ZnO.

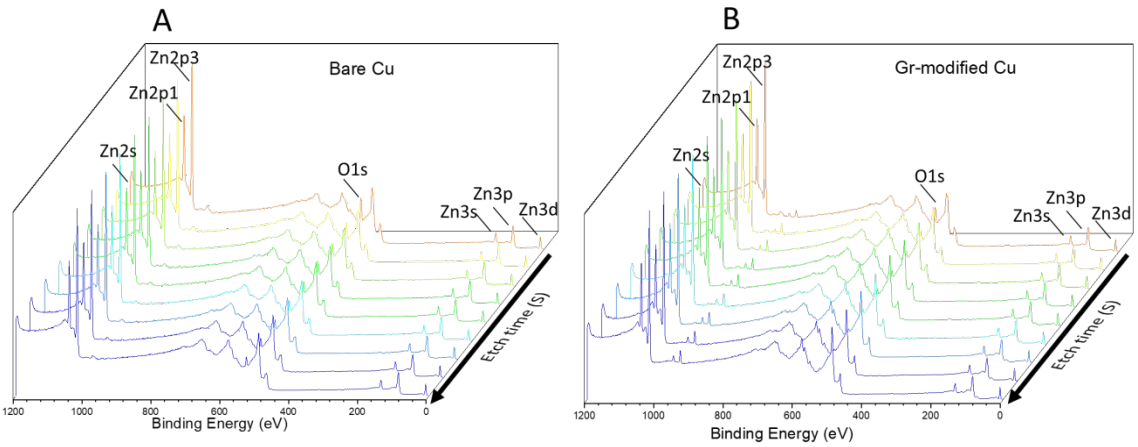

Figure S19. XPS surveys of (A) bare Cu and (B) Gr-modified Cu obtained at each step of the etching.

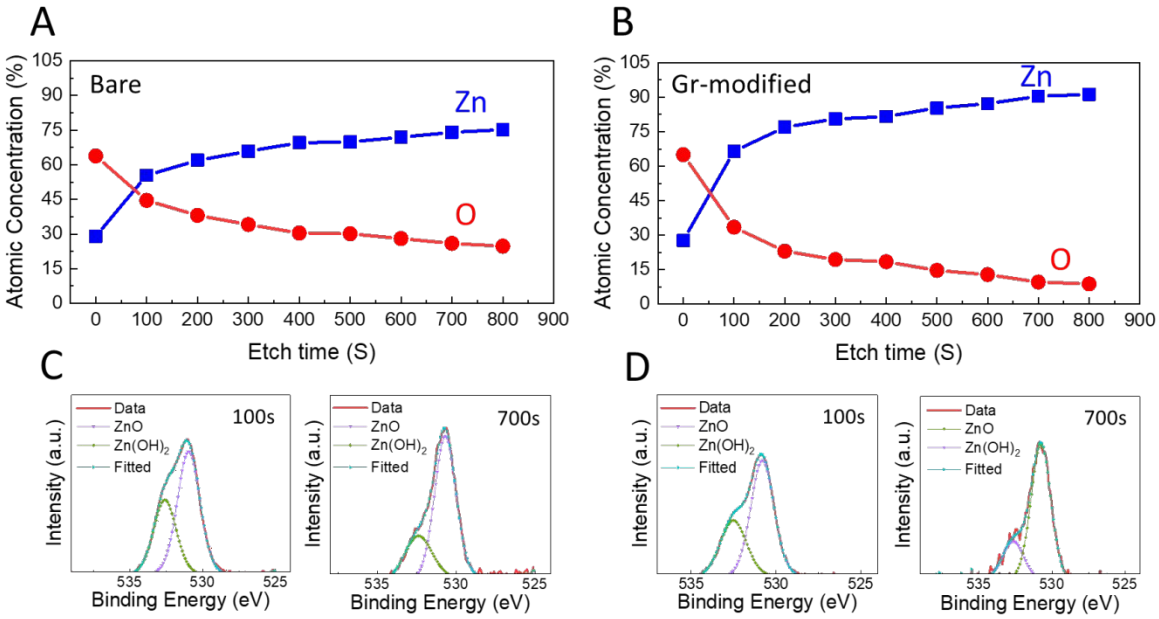

Figure S20. XPS data analysis for bare and Gr-modified samples. Atomic concentration profile of Zn and O for (A) Bare and (B) Gr-modified samples. High resolution fitted XPS spectra of the O binding configurations in case of (C) Bare and (D) Gr-modified Cu electrodes for 1st (left) and 7th (right) sputtering steps, showing the existence of ZnO and $Zn(OH)_2$ compounds.

To study the rate of Zn nucleation on the surface of the bare and the Gr-modified electrodes, we limited the deposition capacity to 0.02 mAh/cm^2 before reversing the current. The voltage-time curve for 6 cycles are shown in Figure S21. Considering that negative voltage denotes metal plating, we highlighted the voltage window, where the Zn deposition can take place. Interestingly, by the limited applied current, Zn could only deposit on the Gr-modified electrode (entering the negative voltage range). Such observations in Figure 4 and Figure S21 denotes to the higher heterogeneous Zn nucleation resistance existing on bare Cu surface.

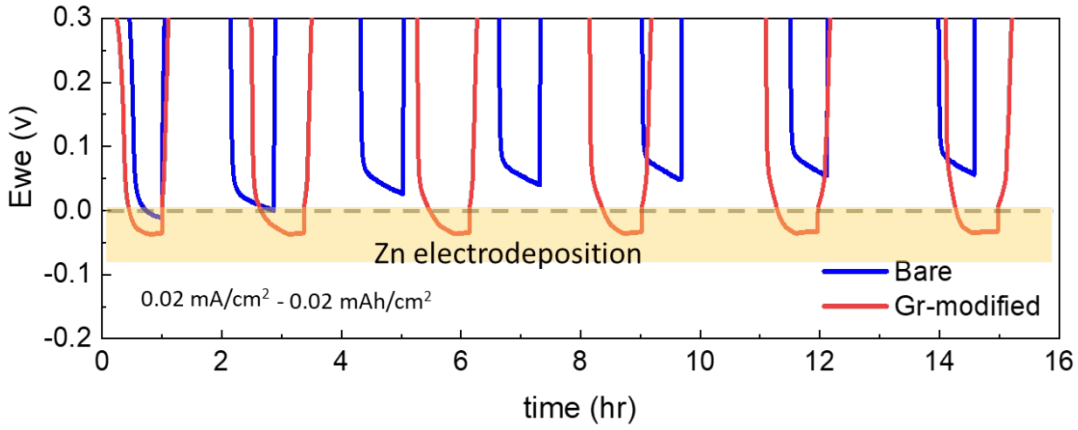

Figure S21. Zn nucleation study on bare and Gr-modified electrodes. 1th to 6th deposition cycles having limited discharge current density of 0.02 mA/cm² for 1hr before reversing the current, showing the Zn electrodeposition mainly in case of Gr-modified electrode.

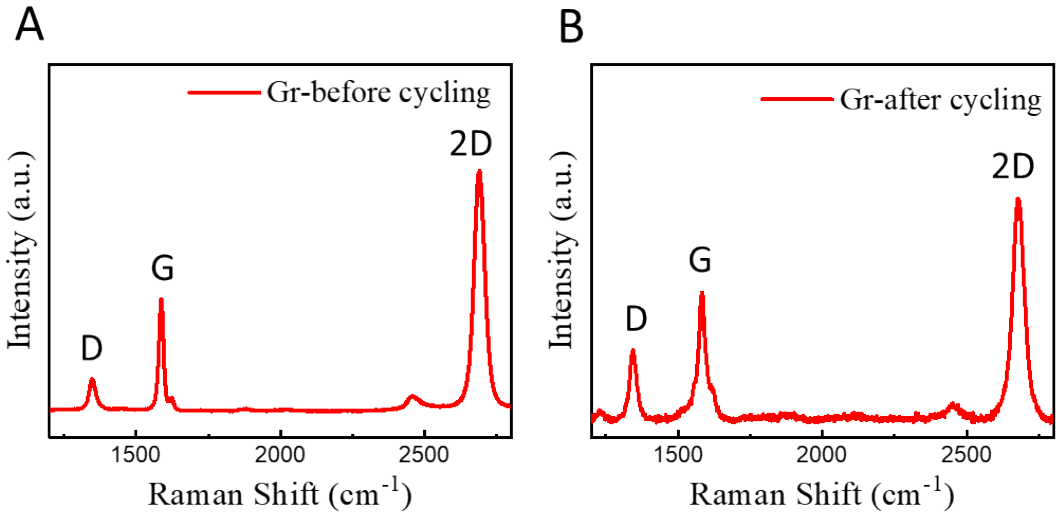

Figure S22. Raman spectra obtained from Gr-modified electrode surface (a) before and (b) after 30 cycling at the fully discharged state.

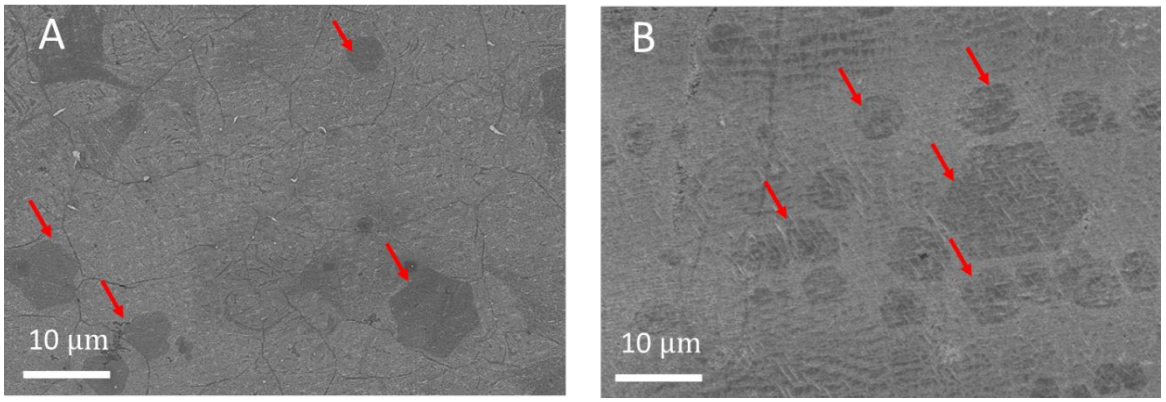

Figure S23. SEM images obtained from Gr-modified electrode (a) before and (b) after 30 cycling at the fully discharged state.

Figure S24 shows the Li behavior in the initial stages of deposition on bare and Gr-modified electrodes at the current density of 2 mA/cm^2. Interestingly, as confirmed by Meng *et al.*[1], we observe a higher nucleation overpotential for Gr-modified sample, which represents the existence of higher Li nucleation barrier. This behavior can explain the role of Gr as physical barrier for nucleation of Li. In addition, the voltage drop follows a stepped pattern in Gr-modified sample, which can be correlated to the lithiation of Gr before reaching to the Cu electrode surface for reduction. This observation has been also detected in other works utilizing Gr as a Li dendrite suppressive film[2].

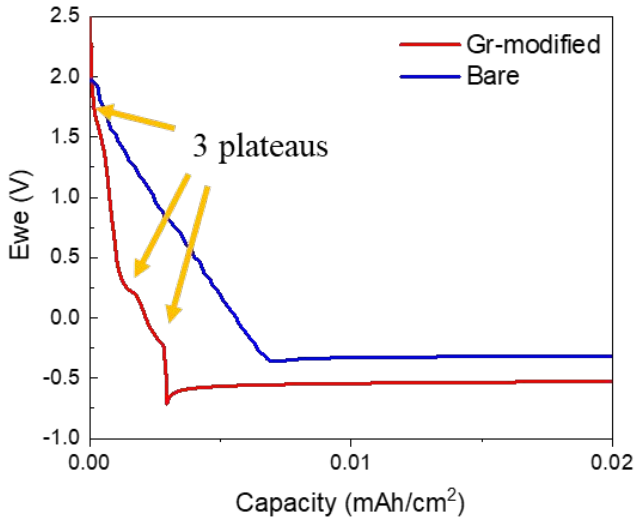

Figure S24. Li nucleation overpotential test for bare and Gr-modified electrodes obtained at the current density of 2mA/cm^2.

In order to visualize the difference in the Li and Zn affinity to Gr and Cu substrates, we utilized the bare Cu and the Gr-modified Cu concurrently as the negative electrode, and Zn/Li metal as the positive electrode in a quartz cell assembly as represented in the schematic in Figure S25A. 2M $ZnSO_4$ electrolyte was used for Zn electrodeposition and 1M $LiPF_6$ in 50/50 EC/DMC electrolyte was used for Li electrodeposition. 4mAh/cm^2 of Zn and/or Li with the current density of 5 mA/cm^2 were deposited on the partially covered Gr electrodes. Interestingly, we observed dissimilar

behavior for Zn versus Li. As shown in the Figure S25B, initial Zn deposition takes place on the Gr-modified electrode, while deposition on the bare Cu is observed only at a few distinct areas which may be the macro-defects introduced on the Cu sheets during the process of Cu foil production. Inversely, the Li-deposition mainly happens on the bare Cu electrode and the defects sites generated on the Gr-modified electrode during the assembly of the electrode in the quartz cell (Figure S25C).

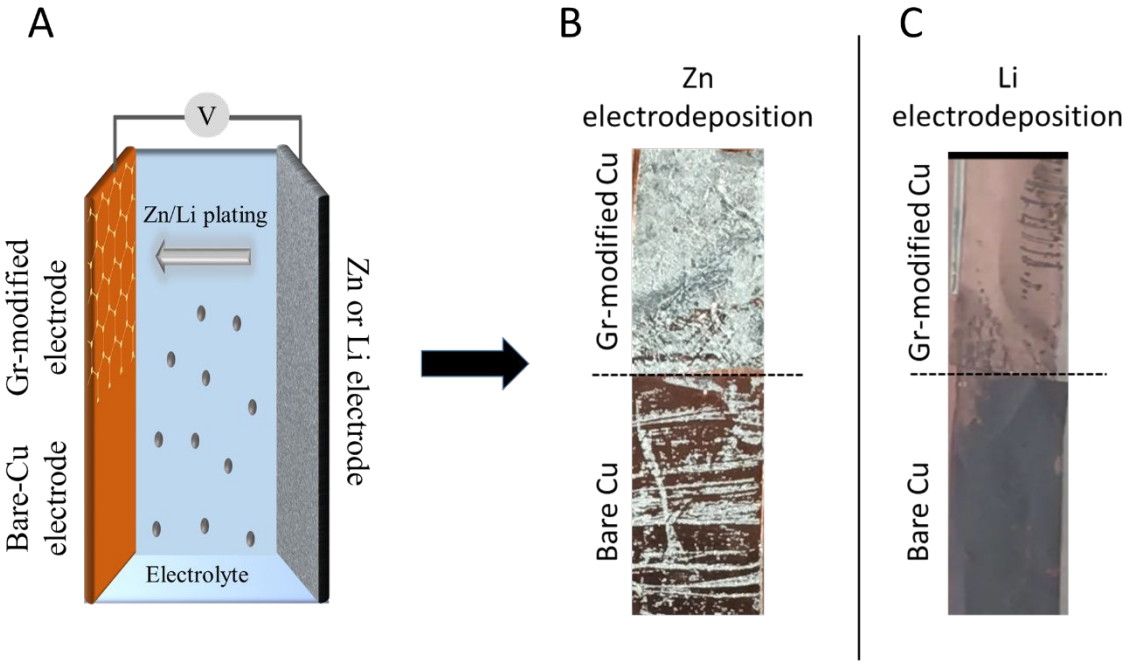

Figure S25. Zincophilicity and lithiophilicity study of Gr vs Cu. (A) Schematic showing the quartz cell assembly used for studying Zn and Li deposition behavior on bare and Gr-modified Cu. The optical image obtained from the partially Gr-covered electrode after 4 mAh/cm^2 of (B) Zn and (C) Li electrodeposition.

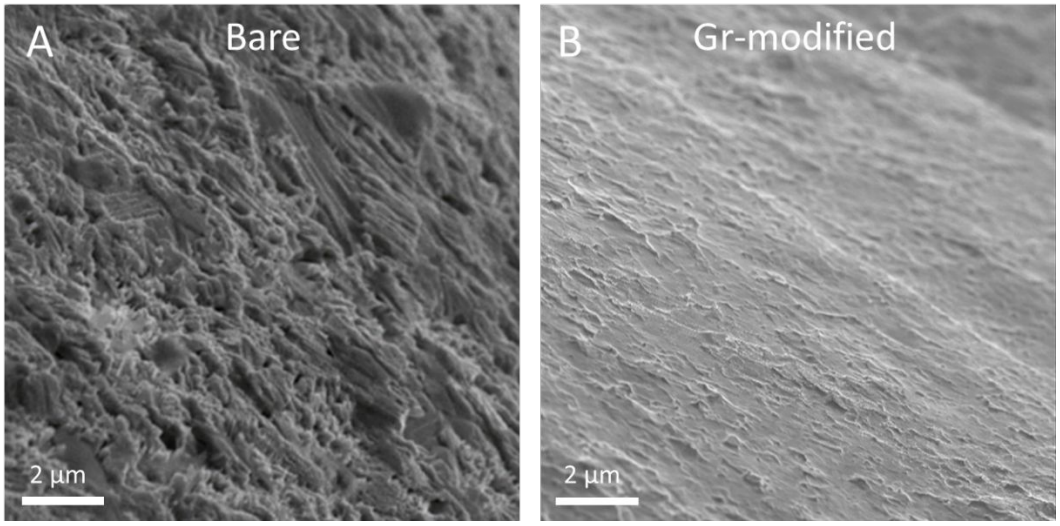

Figure S26. Tilted SEM image obtained from the Zn surface in contact to (A) bare Cu and (B) Gr-modified Cu current collector surface showing a more homogeneous surface for the Gr-modified electrode.

DFT calculations:

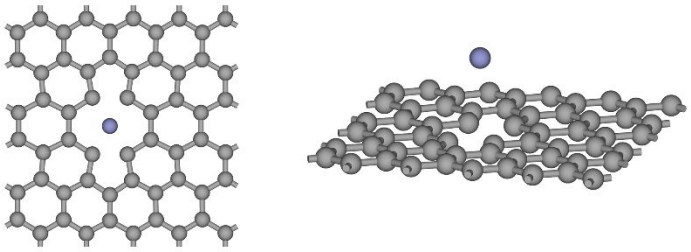

Figure S27. Zn adsorption structures (top and side view) at Gr double vacancy sheet. The adsorption energy is –0.03 eV.

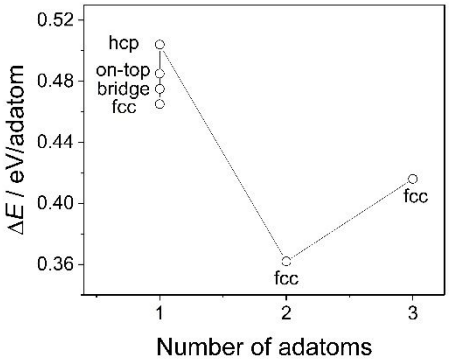

Figure S28. Relative total energy per adatom for Zn adsorption on Zn (0001) surface. Abbreviations on-top, bridge, fcc and hcp denote the corresponding Zn adsorption configuration at the Zn (0001) surface.

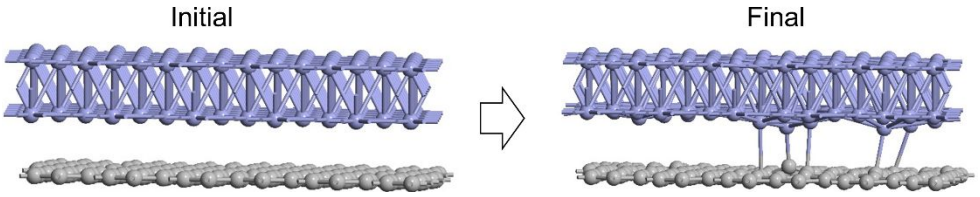

Figure S29. The stability of graphene/Zn interface. DFT results showing interaction between a single graphene sheet with four defects and a Zn (0001) surface.

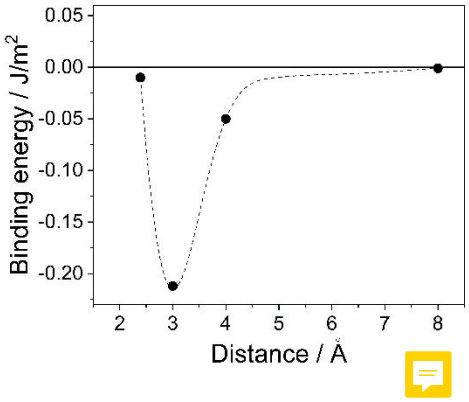

Figure S30. Binding energy as a function of the distance between graphene layer and Zn slab.

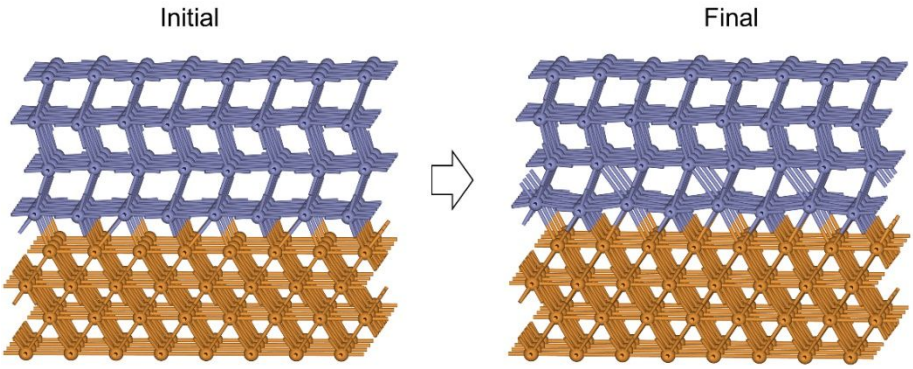

Figure S31. Initial (left) and final optimized (right) interface between Zn (0001) (top) and Cu (200) (bottom) surfaces. Initially both surfaces are strained equally by 2.3 %, however, after the optimization a significant strain is developed at the Zn surface, which may lead to uneven deposition. The interfacial energy as revealed by our DFT calculations is 1.2 J/m^2.

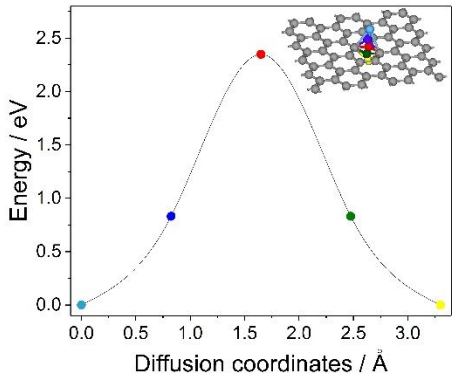

Figure S32. Zn diffusion barrier through Gr single vacancy sheet. The inset picture depicts Zn diffusion path.

References:

1. Meng, Q., Deng, B., Zhang, H., Wang, B., Zhang, W., Wen, Y., Ming, H., Zhu, X., Guan, Y., Xiang, Y., Li, M., Cao, G., Yang, Y., Peng, H., Zhang, H. & Huang, Y. Heterogeneous nucleation and growth of electrodeposited lithium metal on the basal plane of single-layer graphene. *Energy Storage Mater.* **16,** 419–425 (2019).

2. Zhang, R., Wen, S., Wang, N., Qin, K., Liu, E., Shi, C. & Zhao, N. N-Doped Graphene Modified 3D Porous Cu Current Collector toward Microscale Homogeneous Li Deposition for Li Metal Anodes. *Adv. Energy Mater.* **8,** 1–9 (2018).